Cooperative Near-Field Surface Plasmon Enhanced Quantum Dot Nanoarrays

By *Kirsty Leong, Yeechi Chen, David J. Masiello, Melvin T. Zin, Marketa Hnilova, Hong Ma, Candan Tamerler, Mehmet Sarikaya, David S. Ginger,* and *Alex K.-Y. Jen**

Fluorescence from quantum dots (QDs) sandwiched between colloidal gold nanoparticles and lithographically created metal nanoarrays is studied using engineered peptides as binding agents. For optimized structures, a 15-fold increase is observed in the brightness of the QDs due to plasmon-enhanced fluorescence. This enhanced brightness is achieved by systematically tuning the vertical distance of the QD from the gold nanoparticles using solid-specific peptide linkers and by optimizing the localized surface plasmon resonance by varying the geometric arrangement of the patterned gold nanoarray. The size and pitch of the patterned array affect the observed enhancement, and sandwiching the QDs between the patterned features and colloidal gold nanoparticles yields even larger enhancements due to the increase in local electromagnetic hot spots induced by the increased surface roughness. The use of bifunctional biomolecular linkers to control the formation of hot spots in sandwich structures provides new ways to fabricate hybrid nanomaterials of architecturally induced functionality for biotechnology and photonics.

1. Introduction

Hybrid nanosystems composed of inorganic nanostructures and biological molecules have great potential to be used in applications ranging from biotechnology[1–8] to nanoelectronics.[9–13] In particular, hybrid nanosystems composed of noble metals, organic fluorophores, or semiconductor quantum dots (QDs) have been investigated for functionalities in both nanophotonics[14–17] and nanobiomedicine.[18,19] Semiconductor quantum dots offer good photostability, high quantum yield, and spectral tunability.[20,21] When combined with metal nanostructures to form hybrid architectures, both the amount of light absorbed, and the quantum yield of the QD can be altered by the presence of the metal, resulting in enhanced photoluminescence under proper conditions, a phenomenon known as metal enhanced fluorescence (MEF).[22]

MEF attracts interest in the development of nanoscale structures for biological research and clinical diagnosis.[19,23] MEF occurs primarily due to near-field interactions of the excited state fluorophore with the local electric fields of metallic particles induced by incident light. This interaction can enhance the emission of nearby fluorophores in several ways: through enhanced excitation,[24] improved photostability, and/or better quantum yield.[25] Chen and coworkers have studied in detail the fluorescence intensity of dyes attached to silver nanoprisms, leading to the conclusion that the degree of spectral overlap between the plasmon resonance of the nanoparticle and the excitation and emission wavelengths of the emitter play an important role in MEF.[24,26]

The increasing interest in coupling localized surface plasmons in metal nanostructures to explore new phenomena has led to the development of many hybrid nanomaterials.[27–30] Plasmon coupling between nanoparticles results in large electric field enhancements, which have the ability to amplify the fluorescence signal[31,32] and Raman scattering from adsorbed molecules.[33] This concentration of the incident field does not occur homogeneously around the whole metallic nanostructure, but exhibits local maxima such as in the space between two nanoparticles, where the field strength is stronger than that around a single particle.[34,35] These regions of electric field enhancement are termed hot spots, and can be inter-particle junctions or gaps existing between metal nanoparticles.[36] The creation of such hot spots plays a crucial role in surface-enhanced sensitivity of detecting analytes at very low concentrations.

This present work differs from earlier works such as those reported by Pompa et al.,[37] Zhang et al.,[38] and Fu et al.[39] on plasmon enhanced systems. First, we studied the influence of localized surface plasmons on the placement of QDs sandwiched in between interacting nanoparticles to enhance the QD emission. Second, we employ a protein strategy using genetically engineered peptides for the directed self-assembly and immobilization of protein functionalized QDs onto and at controlled distances from the nanostructure surface. This offers a universal platform to generate hybrid nanostructures with high

[*] Dr. M. Hnilova, Prof. H. Ma, C. Tamerler, Prof. M. Sarikaya, Prof. A. K.-Y. Jen
Department of Materials Science and Engineering
University of Washington
Seattle, WA 9819 (USA)
E-mail: ajen@u.washington.edu
K. Leong, Dr. Y. Chen, Dr. D. J. Masiello, Prof. D. S. Ginger
Department of Chemistry
University of Washington
Seattle, WA 98195 (USA)
Dr. M. T. Zin
3M Corporate Research Analytical Laboratory
3M Center, St. Paul, MN 55144 (USA)

DOI: 10.1002/adfm.201000424

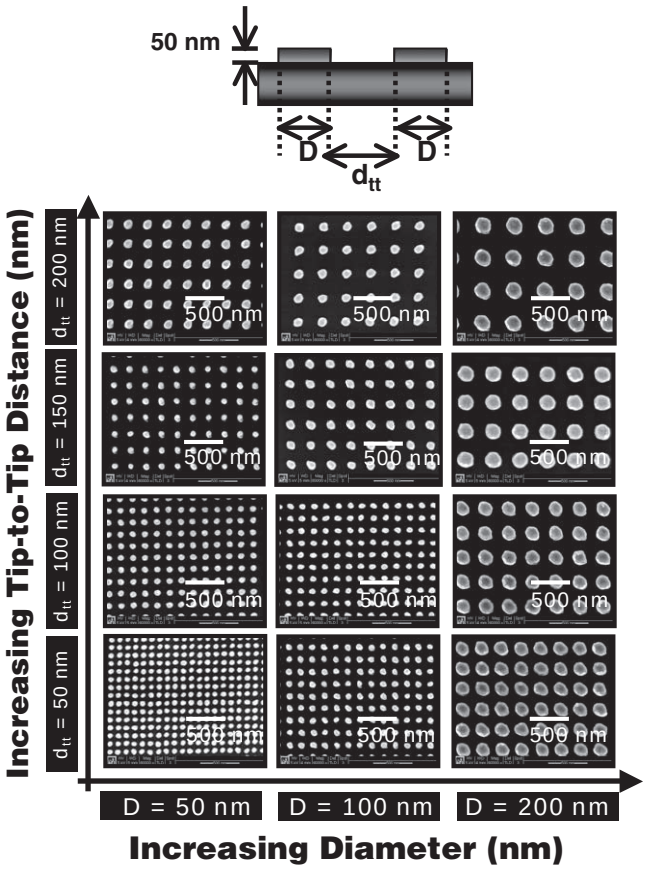

Figure 1. SEM images of EBL fabricated gold nanarrays in 12 different geometric arrangements. The diameter of the nanodisks, *D*, varied from 50 to 100 to 200 nm. The tip-to-tip interparticle spacing, d_{tt}, varied from 50 to 200 nm in 50 nm increments. The height was kept constant at 50 nm.

specificity and nanoscale precision. And third, we also optimize the plasmon-enhanced fluorescence by matching the resonant spectra of the nanoarray with absorption/emission spectra of the fluorophore.

In this study, we examine enhancement of QD photoluminescence when sandwiched into these hot spots. Sandwiched structures where a fluorescent molecule is bridged in between two plasmonic nanoparticles have been shown to increase the intensity of fluorescence and SERS signal.[40–42] Thus, the introduction of hot spots should increase the sensitivity of a system. The design of plasmonic nanodevices relies heavily on the nature of the plasmonic interactions between nanoparticles in the devices that can potentially be fabricated into lab-on-a-chip devices for multiplex sensing capabilities.

2. Results and Discussion

We use 2D gold nanoarrays to probe the effects of plasmon coupling on sandwiched QD nanoarrays. **Figure 1** shows twelve different geometric arrangements of gold nanodisks fabricated using electron-beam (e-beam) lithography (EBL). The heights were kept constant at 50 nm, and three diameters of the gold nanodisks (D = 50, 100, 200 nm) were spaced at four different grating constants (d_{tt} = 50, 100, 150, 200 nm). Each gold nanoarray exhibits strong localized surface plasmon resonances (LSPR) that vary with both the particle diameter and interparticle spacing (**Figure 2a** and 2b). The strong scattering of light reveals the large field enhancement from the collective oscillation of the surface plasmons in noble metal nanostructures. For a given diameter, the LSPR red-shifts as the tip-to-tip spacing increases from 50 to 200 nm.

In effort to model these electromagnetic-scattering experiments on gold nanocylinders, we employ the discrete dipole-dipole approximation (DDA)[43] in conjunction with an analytic model tailored to describing periodic array structures in 1D and 2D.[44] The DDA seeks to discretize the metal target into a collection of point dipoles each induced by the external exciting electric field as well as by the electric-dipole fields of each other. Using the DDA, we display the extinction spectrum of a single gold cylinder as a function of excitation wavelength λ where the incident electric field E is polarized perpendicular to the cylinder axis (Figure 2c). We then use this single nanodisk spectrum to parameterize a model calculation of the extinction of light from an infinite one-dimensional array of gold nanocylinders with periodicity d. In particular, we construct the frequency-dependent polarization p of the array as

$$P(\omega) = \alpha_A(\omega) E(\omega) = \frac{\alpha_C(\omega)}{1 - \alpha_C(\omega) S(\omega)} E(\omega) \quad (1)$$

in terms of the polarizability α_C of the single cylinder and the dipole sum $S(\omega) \equiv S(\omega; r, \theta)$ depending upon the lattice spacing ($r \sim d$) and angle (θ) between lattice axis and field-polarization direction; this sum accounts for the complete and causal electric-dipole coupling between different metallic scattering centers. By approximating α_C to be of the form $\alpha_C(\omega) \approx -A/[\omega - \omega_0 + i\gamma_0]$ and choosing the (positive) amplitude A, resonant frequency ω_0, and width γ_0 to best fit the computed single-cylinder extinction spectrum (~Im α_C) from DDA, we compute the polarization p of the infinite 1D gold nanocylinder array from Equation (1). Application of the optical theorem using p then results in the array extinction spectra displayed (Figure 2c) as a function of λ and d, where the two wave vector of the exciting field is perpendicular to the lattice axis and $\theta = \pi/2$. As in the experiment our calculations reveal that the dipole-plasmon resonance of the array is blue shifted as d decreases. Such an effect is straightforwardly described by the denominator of the array polarizability

$$\alpha_A(\omega) = \frac{-A}{\omega - \omega_0 + i\gamma_0 + AS} = \frac{-A}{\omega - (\omega_0 - \mathrm{Re}\, AS) + i(\gamma_0 + \mathrm{Im}\, AS)} \quad (2)$$

This shows that the resonances of the lattice array are shifted (ω_0 − Re AS) and broadened (γ_0 + Im AS) with respect to those of the single cylinder. Therefore, if Re AS < 0 then the dipole-plasmon resonance of the array is blue shifted with decreasing d due to the long-range and retarded diffractive coupling of individual particle dipole moments. This behavior typically occurs when $D \geq 100$ nm, which is the regime of our observations.

In addition, the scattering spectra of the gold nanoarrays show broad bands with sharp "cliffs" of intense scattering at higher frequencies from their plasmon resonances (Figure 2a). These "cliffs" appear in the visible wavelength region when the

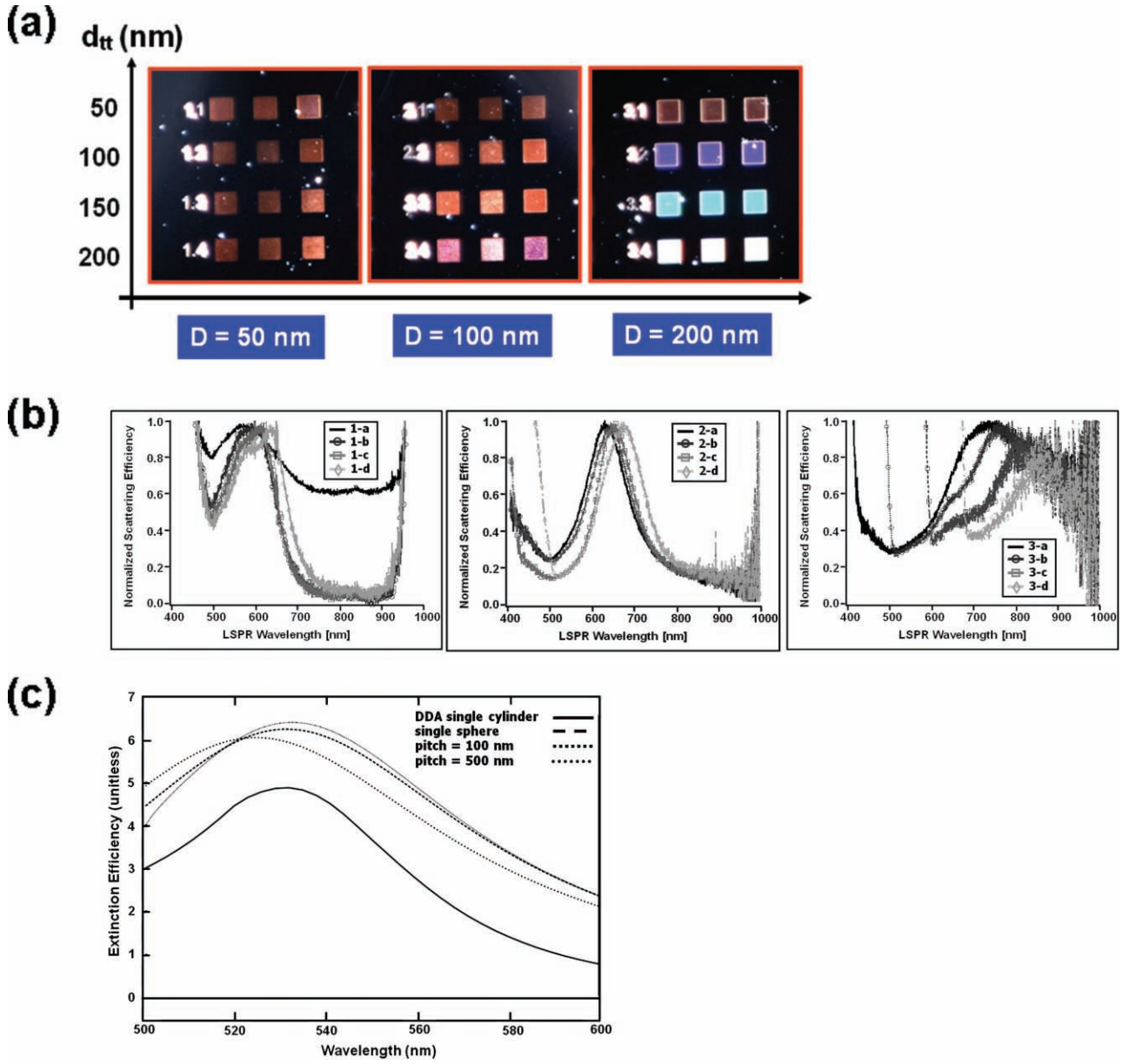

Figure 2. a) Dark-field scattering images of gold nanoarrays. b) Scattering spectra of gold nanoarrays. The scattering spectra 1-a to 1-d correspond to $D = 50$ nm, 2-a to 2-d correspond to $D = 100$ nm, and 3-a to 3-d correspond to $D = 200$ nm. Within each set of spectra, the colors correspond to the nanodisk tip-to-tip distances, blue: $d_{tt} = 50$ nm, green: $d_{tt} = 100$ nm, red: $d_{tt} = 150$ nm, and gold: $d_{tt} = 200$ nm. c) Extinction efficiency spectra of a single gold cylinder under dipole-dipole approximation (black) and sphere (red), and an infinite array of gold cylinders with the following pitch: 100 (green), 150 (blue), 200 (magenta), 250 (yellow), and 500 nm (gray). The diameter of the cylinder and sphere were set at 100 nm with a constant height of 50 nm for the cylinder. Please replace with new figure 2 on the ftp.

center-to-center spacing (pitch) between nanodisks is greater than 250 nm. The on-set of each "cliff" occurs at a wavelength that correlates with the pitch of the nanodisks, but independent of their size. As the pitch increases, the onset wavelength red-shifts; pitches of 250, 300, 350, and 400 nm result in an onset wavelength of 450, 540, 632, and 732 nm, respectively. For pitch distances less than 250 nm, these broad bands are undetected within our detectable range, but we believe these bands could still occur in the ultraviolet region. The intensity of these broad band increases and/or overlaps into the plasmon resonance as the pitch distance increases. As these broad features correlate most closely with the pitch of the nanoarrays, we believe these sharp "cliffs" are related to the diffraction of light by the periodicity of the nanodisks, as will be discussed in a forthcoming paper. In addition to plasmonic effects, diffractive coupling may help enhance the scattering of light and thus the incident electric field.[45,46]

We couple the photoluminescent QDs with the gold nanoarrays by using a peptide-mediated approach. Spacer units composed of genetically engineered polypeptides for inorganic surfaces (GEPIs)[47] and biotin-streptavidin are used to bind QDs onto the gold nanodisks at fixed distances, as depicted in **Figure 3**. GEPIs offer several advantages because of their

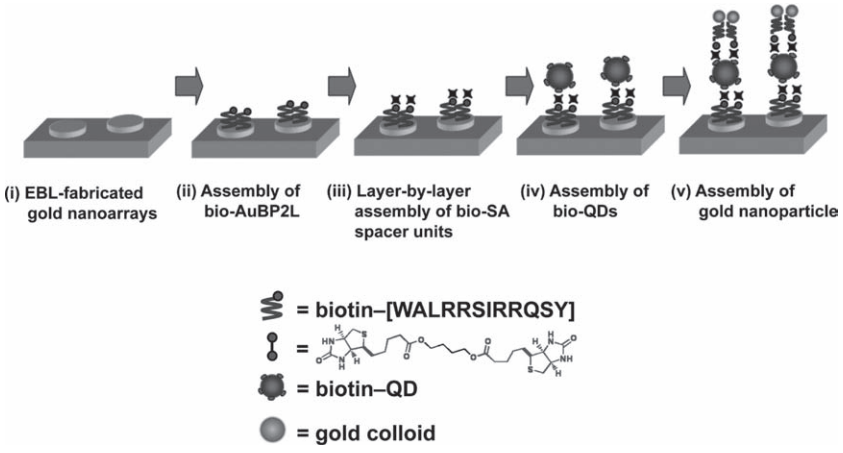

Figure 3. Schematic representation of peptide-mediated fabrication of QD nanoarrays and nanoparticle sandwiched QD nanoarrays.

material specific biomolecular recognition, and potential bifunctional binding to inorganic solid surfaces. The GEPI is a 12 amino acid gold binding polypeptide sequence (AuBP2L = WALRRSIRRQSY) containing a biotin group on the N-terminus of the peptide chain.[48] This peptide-mediated approach allows for the placement of QDs at two well-defined distances from the metal surface (QD–metal distance ≈ 10.50 and 17.50 nm).

The QD emission was measured at QD–metal distances of ~10.50 and ~17.50 nm (**Figure 4a** and 4b). Self-assembled QDs formed a close-packed, optically clear uniform layer, and the extent of aggregation in QD films was negligible. Details on the data calculations can be found in a previous publication.[31] At a QD–metal distance of ~10.50 nm, the emission intensity trend for 50 nm nanoarrays differs from 100 and 200 nm nanoarrays. The QD emission decreases as the tip-to-tip spacing (d_{tt}) increases. On 100 and 200 nm nanoarrays, the QD emission slightly increases as d_{tt} increases from 50 to 100 nm and then decreases. With a larger QD–metal distance of ~17.50 nm, the QD emission is higher than QDs placed ~10.50 nm from the metal surface. As with smaller spacing, QD emission intensity decreases as d_{tt} increases except for those on 50 nm nanoarrays. On these smaller nanodisks, the QD emission is most intense at a d_{tt} spacing of 100 nm, and decreases with larger d_{tt}.

As may be expected,[14,26,49,50] the degree of spectral overlap between the plasmon resonance of the nanoarray and the QD's emission at 605 nm affects the emission intensity of the QD. The nanoarrays where d_{tt} = 50 and 100 nm showed higher QD emission intensity. The plasmon resonances of these nanoarrays range from 589 nm to 675 nm and therefore have a higher degree of spectral overlap compared to nanoarrays where d_{tt} = 150 and 200 nm with the plasmon resonances ranging from 624 to 799 nm. The higher degree of spectral overlap allowed for a stronger field coupling and therefore higher QD emission. It should be also noted that the broad bands with sharp "cliffs" occur at shorter wavelengths and does not overlap with the LSPR when d_{tt} = 50 and 100 nm. The role of diffractive coupling in plasmon enhancement remains unclear and is under investigation.

We further investigated the influence of near-field coupling on the QD's emission due to the formation of hot spots. A sandwich structure was formed by attaching 15 nm diameter gold colloids to the QDs bound to the nanodisk arrays (**Figure 5**). The self-assembly of gold colloids onto the QDs formed a monodispersed layer of approximately twenty colloids on the surface of the quantum dot. With gold colloids placed at an equal distance from the QD bottom supported nanodisk, ~10.50 and ~17.50 nm, the QD's emission showed a further increase (**Figure 6a** and 6b) compared to unsandwiched QD nanoarrays. At an equal gold colloid–QD–metal distance of ~10.50 nm, the QD emission for 50, 100, and 200 nm gold nanoarrays decreases as the d_{tt} increased. At an equal gold colloid–QD–metal distance of ~17.50 nm, the QD emission intensity was higher than gold colloid–QD–metal distance of ~10.50 nm with a similar trend.

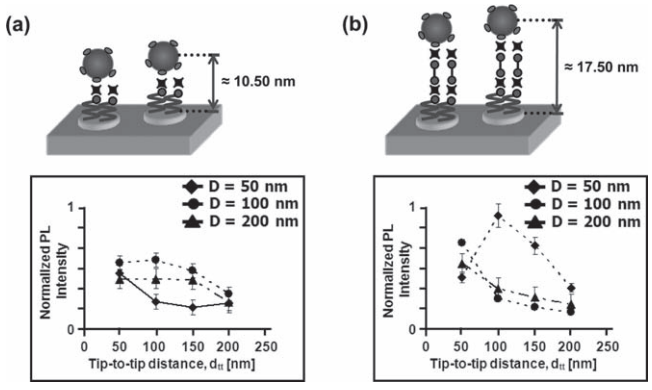

Figure 4. The area normalized photoluminescence (PL) intensity of QD nanoarrays at a QD–metal distance of a) ~10.50 and b) ~17.50 nm, respectively.

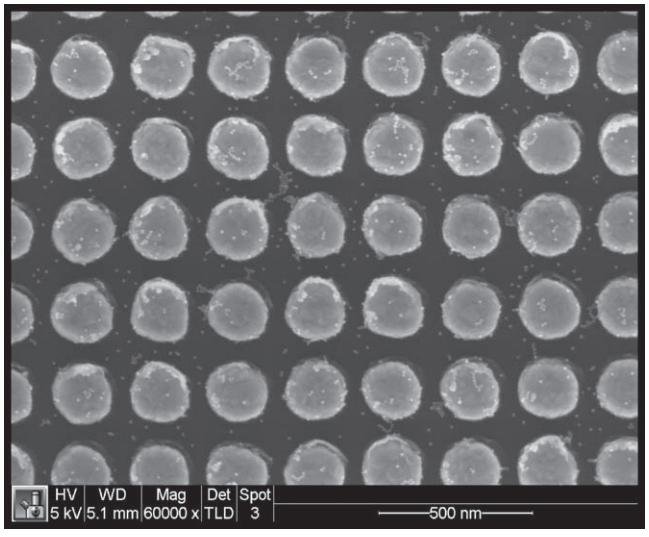

Figure 5. SEM image of gold colloids self-assembled on QDs nanoarrays. The diameter of the nanoarray is 200 nm with a tip-to-tip distance of 50 nm.

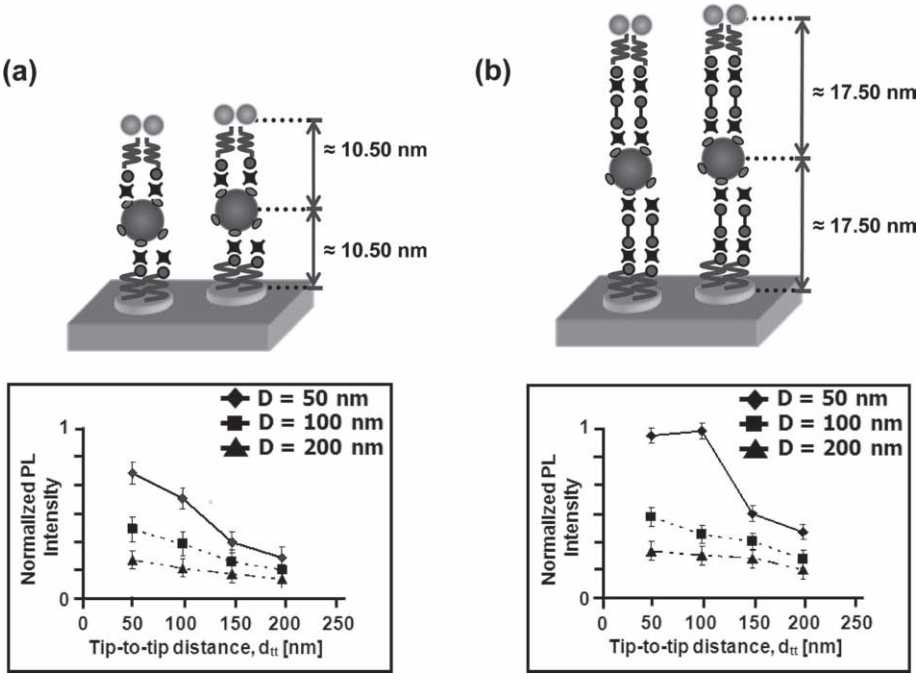

Figure 6. Area normalized PL intensity of nanoparticle sandwiched QD nanoarrays at equal QD–metal distances of a) ~10.50 and b) ~17.50 nm.

These trends suggest that plasmonic coupling between the bottom-supported nanodisks and top self-assembled colloidal gold nanoparticles is an important contributor to the higher QD emission intensity in these systems.

The role of surface roughness in increasing the QD emission was further studied by preparing arrays with different surface roughness without using gold colloids. The EBL process creates nanodisks with an inherent degree of surface roughness. To create more uniformly smooth nanodisks (**Figure 7a**), the nanodisks were thermally annealed (for 8 h at 400 °C) before the QDs were attached on them using molecular linkers (Figure 7b). The QD emission intensity showed a factor of two decrease

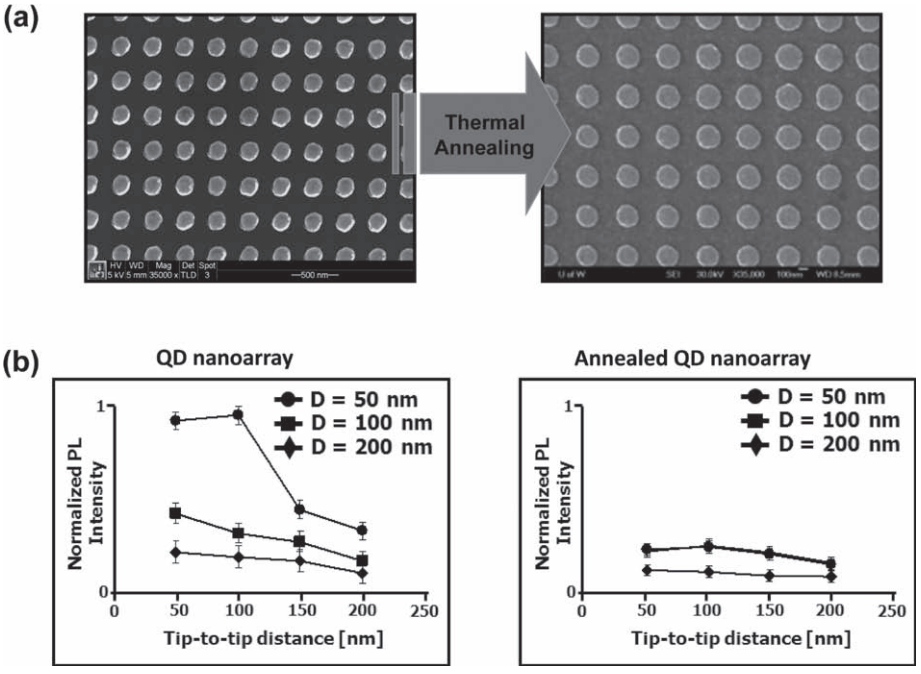

Figure 7. a) SEM image of gold nanoarrays before and after annealing. The gold nanoarrays are more uniform in shape after thermal annealing. b) Normalized PL intensity of QD nanoarrays before and after annealing. The QD emission decreases after annealing the gold nanoarrays.

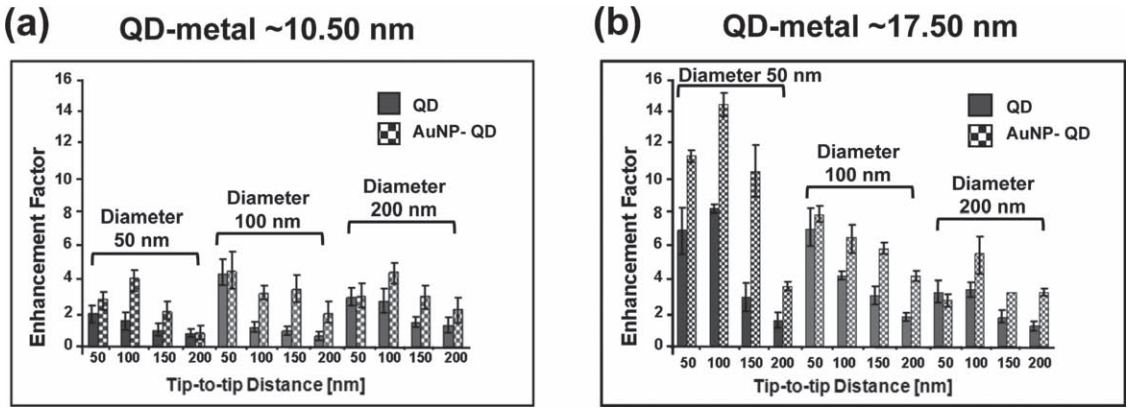

Figure 8. Enhancement factors of QD–metal nanoarrays (solid-filled columns) and nanoparticle sandwiched QD nanoarrays (checker-filled columns) at QD–metal distances of a) ~10.50 and b) ~17.50 nm.

compared to unannealed gold nanoarrays. Surface roughness appears to play a significant role in fluorescence enhancement in these lithographically prepared arrays. Although surface roughness is widely studied in the SERS literature,[51–53] its role is discussed less frequently in the realm of fluorescence enhancement. Our data, both with the annealed substrates and colloidally roughened substrates, confirm that surface roughness is an important variable to consider when evaluating the performance of lithographically defined plasmonic nanostructures in fluorescence applications.

Utilizing roughness in the sandwiched arrays, plasmon-enhanced fluorescence of sandwiched QD nanoarrays was used to obtain a 15-fold increase in the QD emission. The QDs placed at equal distances from the gold metal surface, ~17.50 nm, on the smaller nanoarray showed the highest fluorescence enhancement. Enhancement factors were calculated relative to the emission of a drop-cast thin film of QDs on the nanoarrays. Enhancement factors of QD nanoarrays and sandwiched QD–metal nanoarrays are shown in **Figure 8a** and 8b, respectively. Sandwiched QD nanoarrays showed higher QD enhancements compared to unsandwiched QD nanoarrays. For a given nanodisk diameter, a smaller tip-to-tip spacing (d_{tt} = 50–100 nm) showed higher QD emission due to stronger near-field coupling between neighboring particles within the array, higher degree of spectral overlap between the collective plasmon resonance and QD emission, and the surface roughness of the nanodisks.

3. Conclusion

In summary, we used peptide-mediated assembly to create hot spots between lithographic nanodisks and colloidal particles, and confirmed that surface roughness can play important role in the fluorescence enhancement. The peptide-linked structures allowed the QDs to be placed reproducibly at the hot spots in the roughened structures, and QDs placed in optimally sandwiched metal nanoarrays exhibited a 15-fold enhancement of the QD photoluminescence, as compared to QDs simply bound to the nanodisks alone. Although cylinders are not the most appropriate shapes for highest enhancement factors, we demonstrate a proof-of-concept study of sandwiched QD structures, and we will design other nanostructures in future publication. This enhanced QD emission suggests that such a synergetic combination of spectral overlap and surface roughness should enable precise control necessary to produce highly integrated multifunctionalities into hybrid nanoassemblies potentially for a diverse range of nano- and biotechnology applications.

4. Experimental Section

Materials: Sulfuric acid, hydrogen peroxide (30%), poly(methyl methacrylate), isopropyl alcohol, methyl-isobutylketone, streptavidin, chlorobenzene, and ammonia hydroxide (28.0%–30.0% NH_3) were purchased from Aldrich (St. Louis, MO) and used as received unless stated otherwise. Absolute (200 proof) ethanol was purchased from Aaper Alcohol and Chemical Company and used in preparation of thiol solutions. 1–4 dibiotinylbutane was synthesized in our laboratory. Gold colloids with a diameter of 10 nm were purchased from Ted Pella, Inc (City, State). *L*-AuBP2 was synthesized by the Sarikaya group. Biotin-labeled quantum dot 605 (bio-QD) and Dulbecco's phosphate buffered saline (PBS) without calcium and magnesium were purchased from Invitrogen (Carlsbad, CA). Deionized water for rinsing was produced with a NANOpure Diamond purification unit (Barnstead International, Dubuque, IA) and had a resistivity of ~15 MΩ cm^{-1}.

Gold Nanoarray Fabrication: Boron-doped Si (100) wafers of test grade (diameter, 100 mm; resistivity, 1–10 Ω cm^{-1}; thickness, 525 (≠ 50 μm) were purchased from Silicon Sense (Nashua, NH). In preparation for EBL, Si wafers were fractured into small substrates and cleaned in a two-step procedure: i) piranha etch, 3:1 H_2SO_4:H_2O_2(30%) for 1 h; ii) base treatment, 5:1:1 H_2O:NH_4OH:H_2O_2 (30%) with sonication for 1 h. Thin films (110–140 nm) of poly(methyl methacrylate) (PMMA; 950k; diluted in chlorobenzene) resist were spin-coated on Si (001) substrates, annealed at 180 °C on a hot plate for 2 min to improve the film uniformity, and then exposed to an electron beam at an accelerating voltage of 30 keV. EBL was performed using a field emission scanning electron microscope (SEM; FEI Sirion, Hillsboro, OR) that has been equipped a nanolithography system. A nanometer pattern generation system (NPGS), developed by JC Nabity Lithography System (Bozeman, MT), was used to design and direct-write nanoarrays. After the e-beam exposure, substrates were developed in a 1:3 mixture of methyl-isobutylketone/isopropanol (MIBK/IPA) at room temperature for ~70 s and baked at 90 °C in a vacuum oven for 30 min. The samples were checked by SEM to assess the integrity of nanopatterned PMMA films before the metallization process. Metal (5 nm of chromium and 50 nm of gold) was deposited onto nanopatterned PMMA films by electron-beam evaporation (SEC 6000, CHA Industries)

under a high vacuum with base pressure of ~1×10^{-6} Torr. The deposited thickness and deposition rate were measured by a quartz crystal microbalance (QCM). The deposition rate was maintained at ~0.1 nm s^{-1} to achieve high-quality gold nanostructures with smooth surfaces. In the lift-off step, gold nanoarrays were obtained by dissolving the PMMA resist in acetone overnight (~24 h).

Self-Assembly of Linker Molecules: The gold-binding polypeptide, referred to as *l*-AuBP2, with a peptide sequence WALRRSIRRQSY was synthesized using standard Fmoc solid-phase peptide synthesis technique, detailed synthesis and characterization are published elsewhere.[48] Biotin (bio) was chemically linked to the *N*-terminus of the peptide to create a bifunctional bimolecular construct which serves as a binder for specific adsorption to the gold substrate as well as a receptor for controlling the self-assembly of biotin functionalized CdSe–ZnS QDs (bio-QDs) through biotin-streptavidin interaction. Bio-*l*-AuBP2 was self-assembled onto the gold nanoarrays for 2 h, followed by the sequential attachment of spacer units using streptavidin and 1,4-dibiotinylbutane for a reaction time of 35 min between each attachment. After each self-assembling, the substrate was thoroughly rinsed using PBS, DI water, and lastly ethanol, then dried under nitrogen gas.

Self-Assembly of CdSe-ZnS QDs: Biotin conjugated QDs (bio-QDs) were diluted to a working solution of 10 nM using PBS. The EBL nanopatterned substrate was immersed into the diluted bio-QD solution for 45 min and then thoroughly rinsed with PBS buffer, DI water, and dried using N_2 gas.

Surface Characterization: SEM images were obtained from the EBL fabricated substrates using a FEI Sirion SEM at the University of Washington NanoTechnology User Facility at an accelerating voltage of 5 keV. Atomic force microscopy (AFM) images from experiments performed on gold substrates were carried out in air under ambient conditions (ca. 40%–50% relative humidity, 25 °C temperatures) on a Digital Instruments Nanoscope III Multimode AFM (Veeco Inc., Santa Barbara, CA) using tapping mode at a scan rate of 0.5–1.0 Hz. Silicon cantilevers with spring constants ranging from 12 to 103 N m^{-1} were used. Image resolution was 512×512 pixels. Cross-sectional analysis was performed using an algorithm contained in the AFM software. Optical microscopy/spectroscopy were performed using a Nikon TE-2000 inverted microscope fitted with a transmitted darkfield condenser and a 50X objective (Nikon Plan RT, NA 0.7, CC 0–1.2) with an intermediate 1.5× lens (total magnification 75×). The microscope output was either directed to a thermoelectrically-cooled color CCD camera (Diagnostic Instruments, FX1520) or a fiber optic cable (diameter = 200 µm, UV-vis transmission, Ocean Optics, Dunedin, FL) coupled to a portable charge coupled device spectrometer (USB2000, Ocean Optics). A standard tungsten halogen lamp was used for transmitted light dark-field illumination, and unpolarized white light illumination by a metal halide lamp (EXFO X-Cite 120) was used for epi-fluorescence illumination. A lamp reference spectrum was obtained by measuring the scattered white light from a laboratory wipe. A background spectrum was obtained by measuring the focused, scattered white light from an empty region on the substrate. The scattered light spectrum from each nanoarray minus the backgrounds spectrum was divided by the lamp reference spectrum to give the scattering efficiency (and LSPR peak). Fluorescence intensities were obtained for each nanoarray by imaging the substrates with a custom quantum dot 605 filter set. The QDs were excited with a 405/20 nm bandpass filter and emission intensities recorded between 595 and 615 nm. The filter set, purchased from Chroma Technology Corp (Rockingham, VT), reduced background signal to less than 1% of the sample signal.

Acknowledgements

This work is supported by the National Science Foundation's NSF-STC program and GEMSEC (Genetically Engineered Materials Science and Engineering Center) through the NSF-MRSEC program. A.K.-Y. Jen thanks the Boeing-Johnson Foundation for financial support. Materials were prepared in GEMSEC facilities and the instrumentation for electron-beam lithography was provided by the Nanotechnology User Facility (NTUF), a member of the National Nanotechnology Infrastructure (NNIN). D.S. Ginger and Y. Chen thank AFOSR for additional support.

Received: March 6, 2010
Revised: April 13, 2010
Published online: July 7, 2010

[1] K. Aslan, I. Gryczynski, J. Malicka, E. Matveeva, J. R. Lakowicz, C. D. Geddes, *Curr. Opin. Biotech.* **2005**, *16*, 55.
[2] C. Tamerler, M. Sarikaya, *ACS Nano* **2009**, *3*, 606.
[3] O. Salata, *J. Nanobiotechnol.* **2004**, *2*, 1.
[4] J. Ziauddin, D. M. Sabatini, *Nature* **2001**, *411*, 107.
[5] K.-B. Lee, S.-J. Park, C. A. Mirkin, J. C. Smith, M. Mrksich, *Science* **2002**, *295*, 1702.
[6] C. M. Niemeyer, *Angew. Chem. Int. Ed.* **2003**, *42*, 5796.
[7] G. T. Lu, Y. Huang, *J. Mater. Sci.* **2002**, *37*, 2305.
[8] Q. Zhou, S. Wang, X. Fan, R. Advincula, J. Mays, *Langmuir* **2002**, *18*, 3324.
[9] X. Ji, J. E. Hampsey, Q. Hu, J. He, Z. Yang, *Chem. Mater.* **2003**, *15*, 3656.
[10] S. Guo, S. Dong, *Trends Anal. Chem.* **2009**, *28*, 96.
[11] A. N. Shipway, E. Katz, I. Willner, *ChemPhysChem* **2000**, *1*, 18.
[12] C. R. Kagan, C. B Murray, M. Nirmal, M. G. Bawendi, *Phys. Rev. Lett.* **1996**, *76*, 1517.
[13] Y. Huang, X. Duan, C. M. Lieber, *Small* **2005**, *1*, 142.
[14] Y. Chen, K. Munechika, D. S. Ginger, *MRS Bull.* **2008**, *33*, 536.
[15] C.-Y. Zhang, H-C. Yeh, M. T. Kuroki, T-H. Wang, *Nat. Mater.* **2005**, *4*, 826.
[16] R. Sinha, G. J. Kim, S. Nie, D. M. Shin, *Mol. Cancer Ther.* **2006**, *5*, 1909.
[17] E. R. Goldman, E. D. Balighian, H. Mattoussi, M. K. Kuno, J. M. Mauro, P. T. Tran, G. P. Anderson, *J. Am. Chem. Soc.* **2002**, *124*, 6378.
[18] M. Bruchez Jr., M. Moronne, P. Gin, S. Weiss, A. P. Alivisatos, *Science* **1998**, *281*, 2013.
[19] I. L Medintz, H. T. Uyeda, E. R. Goldman, H. Mattoussi, *Nat. Mater.* **2005**, *4*, 435.
[20] C. J. Murphy, *Anal. Chem.* **2002**, *74*, 520.
[21] W. J. Parak, D. Gerion, T. Pellegrino, D. Zanchet, C. Micheel, S. C. Williams, R. Boudreau, M. A. Le Gros, C. A. Larabell, A. P. Alivisatos, *Nanotechnology* **2003**, *14*, 15.
[22] J. R. Lakowicz, in *Principles of Fluorescence Spectroscopy*, 3rd ed., Kluwer Academic/Plenum Publishers, New York **2006**.
[23] *A Practical Guide to Technology for Quantitative Real-Time Analysis: Fluorescent and Luminescent Probes for Biological Activity* (Ed.: W. Mason) Academic Press, New York **1999**
[24] Y. Chen, K. Munechika, I. Jen-La Plante, A. M. Munro, S. E. Skrabalak, Y. Xia, D. S. Ginger, *Appl. Phys. Lett.* **2008**, *93*, 053106.
[25] C. D. Geddes, J. R. Lakowicz, *J. Fluoresc.* **2002**, *12*, 121.
[26] K. Munechika, A. Tillack, Y. Chen, D. S. Ginger, unpublished.
[27] I. Gryczynski, J. Malicka, Y. Shen, Z. Gryczynski, J. R. Lakowicz, *J. Phys. Chem. B* **2002**, *106*, 2191.
[28] K. Aslan, J. Huang, G. M. Wilson, C. D. Geddes, *J. Am. Chem. Soc.* **2006**, *128*, 4206.
[29] P. Pramod, K. G. Thomas, *Adv. Mater.* **2008**, *20*, 4300.
[30] S. K. Ghosh, T. Pal, *Chem. Rev.* **2007**, *107*, 4797.

[31] M. T. Zin, K. Leong, N.-Y. Wong, H. Ma, M. Sarikaya, A. K.-Y. Jen, *Nanotechnology* **2009**, *20*, 015305.
[32] P. P. Pompa, L. Martiradonna, A. Della Torre, L. Carbone, L. L. del Mercato, L. Manna, M. De Vittorio, F. Calabi, R. Cingolani, R. Rinaldi, *Sens. Actuators B* **2007**, *126*, 187.
[33] A. Gopinath, S. V. Boriskina, B. M. Reinhard, L. Dal Negro, *Opt. Express* **2009**, *17*. 3741.
[34] K. L. Kelly, E. Coronado, L. L. Zhao, G. C. Schatz, *J. Phys. Chem. B* **2003**, *107*, 668.
[35] E. Hao, S. Li, R. C. Bailey, Z. Zou, G. C. Schatz, J. T. Hupp, *J. Phys. Chem. B* **2004**, *108*, 1224.
[36] M. Futamata, *Faraday Discuss.* **2006**, *132*, 45.
[37] P. P. Pompa, L. Martiradonna, A. Della Torre, F. Della Sala, L. Manna, M. De Vittorio, F. Calabi, R. Cingolani, R. Rinaldi, *Nat. Nanotechnol.* **2006**, *1*, 126.
[38] J. Zhang, J. Malicka, I. Gryczynski, J. R. Lakowicz, *J. Phys. Chem. B* **2005**, *109*, 7643.
[39] Y. Fu, J. R. Lakowicz, *J. Phys. Chem. B* **2006**, *110*, 22557.
[40] A. Bek, R. Jansen, M. Ringler, S. Mayilo, T. Klar, J. Feldmann, *Nano Lett.* **2008**, *8*, 485.
[41] C. Orendorff, A. Gole, T. K. Sau, C. J. Murphy, *Anal. Chem.* **2005**, *77*, 3261.
[42] L. Guerrini, J. V. Garcia-Ramos, C. Domingo, S. Sanchez-Cortes, *J. Phys. Chem. C* **2008**, *112*, 7527.
[43] B. T. Draine, P. J. Flatau, *J. Opt. Soc. Am.* **1994**, *A11*, 1491.
[44] S. Zou, N. Janel, G. C. Schatz, *J. Chem. Phys.* **2004**, *120*, 10871.
[45] J. Dostálek, A. Kasry, W. Knoll, *Plasmonics* **2006**, *2*, 97.
[46] J. G. Rivas, G. Vecchi, V. Giannini, *New J. Phys.* **2008**, *10*, 105007.
[47] M. Sarikaya, C. Tamerler, K. Schuten, A. K-Y. Jen, F. Baneyx, *Nat. Mater.* **2003**, *2*, 577.
[48] M. Hnilova, E. E. Oren, U. O. S. Seker, B. Wilson, S. Collino, J. S. Evans, C. Tamerler, M. Sarikaya, *Langmuir* **2008**, *24*, 12440.
[49] Y. Chen, K. Munechika, J. M. Smith, D. S. Ginger, *Nano Lett.* **2007**, *7*, 690.
[50] K. Munechika, Y. Chen, J. M. Smith, D. S. Ginger, in *Metal Enhanced Fluorescence* (Ed.: C. D. Geddes), Wiley, New York **2010**.
[51] S. Kruszewski, *Surf. Interface Anal.* **2004**, *21*, 830.
[52] C. L. Haynes, R. P. Van Duyne, *J. Phys. Chem. B.* **2003**, *107*, 7426.
[53] S. G. Schultz, M. Janik-Czachor, R. P. Van Duyne, *Surf. Sci.* **1981**, *104*, 419.